Imprints of evaporative conditions and vegetation type in diurnal temperature variations

Annu Panwar[1], Maik Renner[1,2], Axel Kleidon[1]

[1] Biospheric Theory and Modeling group, Max Planck Institute for Biogeochemistry, Jena, 07745, Germany

[2] now at: Flood Monitoring Centre, Brandenburg State Office for Environment, Müllroser Chaussee 50, 15236 Frankfurt (Oder), Germany

Correspondence to: Annu Panwar (apanwar@bgc-jena.mpg.de)

Abstract. Diurnal temperature variations are strongly shaped by the absorption of solar radiation, but evaporation, or the latent heat flux, also plays an important role. Generally, evaporation cools. Its relation to diurnal temperature variations, however, is unclear. This study investigates the diurnal response of surface and air temperatures to evaporative conditions for different vegetation types. We use the warming rate, defined as the increase of temperature in response to absorbed solar radiation in the morning, and evaluate how it changes with evaporative fraction, which is an indicator of the evaporative conditions. Results for 51 FLUXNET sites show that the warming rate of air temperature carries very weak imprints of evaporative fraction across all vegetation types. However, the warming rate of surface temperature is strongly sensitive to evaporative fraction with a value of $\sim 23 \times 10^{-3}$ K (W m^{-2})$^{-1}$, indicating stronger evaporative cooling for moister conditions. Contrarily, warming rates of surface and air temperatures are similar at forest sites and carry literally no imprints of evaporative fraction. We explain these contrasting patterns with an analytical surface energy balance model. The derived expressions reproduce the observed warming rates and their sensitivity to evaporative fraction in all vegetation types. Multiplying the warming rate with daily maximum solar radiation gives an approximation for the diurnal surface temperature range (DT$_s$R). We use our model to compare the individual contributions of solar radiation, evaporative conditions and vegetation (by its aerodynamic conductance) in shaping DT$_s$R and show that the high aerodynamic conductance of forests reduces DT$_s$R substantially more (-56%) than evaporative cooling (-22%). We further show that the strong diurnal variation of aerodynamic conductance ($\sim$2.5 times of the mean across vegetation types) reduces DT$_s$R by $\sim$35 % in short vegetation and savanna, but only by $\sim$22% in forests. We conclude that diurnal temperature variations may be useful to predict evaporation for short vegetation. In forests, however, the diurnal variations in temperatures are mainly governed by their high aerodynamic conductance resulting in negligible imprints of evaporative conditions.

1 Introduction

Temperature is one of the most widely monitored variables in meteorology. Besides being important for our day-to-day activities, temperature serves as a primary attribute for the understanding of Earth system processes. The diurnal variation of temperature is considered informative in climate science, as described by the diurnal temperature range (DTR), which is basically the difference between daily

maximum and minimum temperatures. Information on the diurnal temperature range has facilitated a broad spectrum of research including agriculture, health welfare, climate change and ecological studies.

Over land, the diurnal variation of temperature is mainly driven by the solar energy input (Bristow and Campbell, 1984). Liu et al., (2004) shows a high correlation of 0.88 between the annual solar radiation and DTR in China. Likewise, Makowski et al., (2009) found their annual correlation to be 0.87 for Europe. Their obvious and still intricate association is also important in determining the influence of solar dimming and brightening on diurnal temperature variations (Wang and Dickinson, 2013; Wild, 2005).

Solar radiation is the dominant, but not the only factor shaping the diurnal temperature. Available energy at the surface is partitioned into latent and sensible heat flux. A higher latent heat flux signifies higher evaporation, which reduces the temperature through evaporative cooling, an effect that can be seen in sensitivity simulations with a global climate model to land evaporation (Shukla and Mintz, 1982). Another climate model-based analysis (Mearns et al., 1995) shows that differences in evaporation explain 52% of the variance in DTR in the summer season for the USA. Similarly, climate model simulations also show the high sensitivity of DTR to evaporation especially in the summer season when evaporation is not energy limited (Lindvall and Svensson, 2015). Consequently, methods to estimate evaporation use air temperature (Blaney and Criddle, 1950; Hargreaves and Samani, 1985; Thornthwaite, 1948) and remotely sensed surface temperature (Anderson et al., 2012; Boegh et al., 2002; Jackson et al., 1999; Kustas and Norman, 1999; Price, 1982; Su et al., 2007). Most of the surface energy balance-based estimates of evaporation use DTR as an input (Baier and Robertson, 1965; Vinukollu et al., 2011; Yao et al., 2013).

Clouds and precipitation are also important factors that determine DTR (Dai et al., 1999; Stenchikov and Robock, 1995). One can exclude their contribution to some extent by considering only clear sky days to distinctly identify the role of evaporative conditions on DTR. Furthermore, the partitioning of the turbulent heat fluxes into sensible and latent heat is also influenced by vegetation type. Taller vegetation has a higher aerodynamic conductance that facilitates mass and heat exchange between land and atmosphere (Jarvis and McNaughton, 1986). The greater aerodynamic conductance in forests reduces their DTR by reducing their maximum temperatures (Bevan et al., 2014; Gallo, 1996; Jackson and Forster, 2010). Few studies captured the impact of aerodynamic properties of vegetation on temperature, for example, in terms of the decomposed temperature metric theory (Juang et al., 2007; Luyssaert et al., 2014) and the theory of intrinsic biophysical mechanism (Lee et al., 2011a; Zhao et al., 2014a). Generally, the lower temperatures of forests are associated with their mean evaporative environment, although this may be affected by periods of dry and moist conditions.

In this study, we investigate how the diurnal variation in surface and air temperature responds to changes in evaporative conditions in different vegetation types. Clearly, DTR is not independent of solar radiation, which is why we develop an alternative indicator, the warming rate (Panwar et al., 2019), that eliminates the contribution of solar radiation. To illustrate this, the observed normalized

diurnal air and surface temperatures are plotted against absorbed solar radiation for a cropland and forest site in Figure 1. Surface temperature is obtained from upwelling longwave radiation from the surface and air temperature above the canopy, usually measured at 2 m height. The diurnal evolution of temperature is mainly governed by the absorbed solar radiation (R_s); this is discernible from the linear increase in the morning (20 W m^{-2} $\leq$ R_s $\leq$ $R_{s,max}$), as described by the slope. This dependence is accounted for by what we refer to as the warming rate, the increase in temperature due to a unit increase in the absorbed solar radiation, expressed as the derivative dT_a/dR_s for air temperature and dT_s/dR_s for surface temperature with units of K (W m^{-2})$^{-1}$. One can approximate the warming rate by the ratio of DTR to maximum solar radiation, $R_{s,max}$, so that the warming rate can be seen as an efficient characteristic that captures effects on DTR that are not caused by solar radiation. In this study, we use linear regressions of observed data from the morning to noon to calculate warming rates.
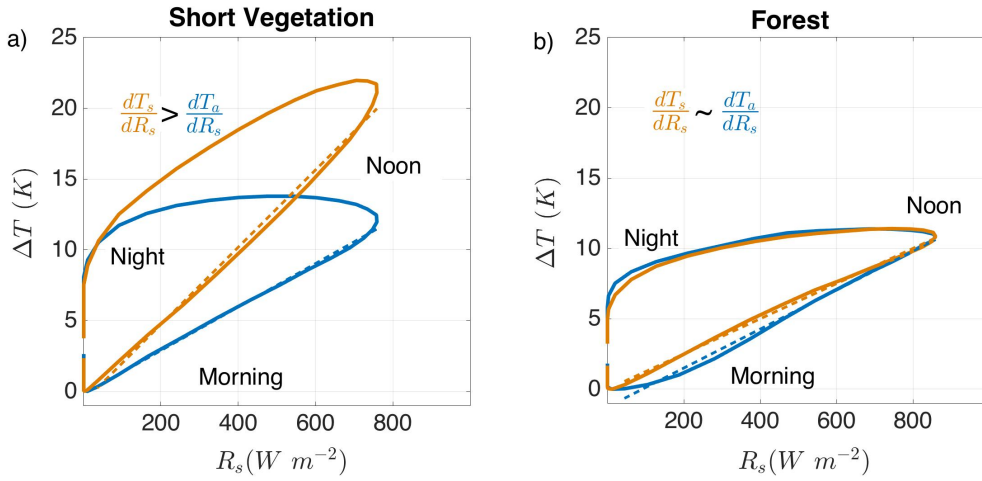
Figure 1 Mean diurnal hysteresis formed by plotting the normalized diurnal temperature ($\Delta T = T - T_{min}$) against absorbed solar radiation (R_s) for summer clear sky days. Surface temperature (T_s) is depicted in orange and air temperature (T_a) in blue. (a) A short vegetation cropland site (US-ARM) in Southern Great Plains Lamont OK, United States. (b) A forest site (CA-TP4) in Ontario, Canada. The dashed lines are the linear regression of the observations falling in the morning slope of the hysteresis that corresponds to the warming rate of air (dT_a/dR_s) and surface temperature (dT_s/dR_s).

The temperature warming rate provides insights on the effects of vegetation on the diurnal variation of temperatures. Figure 1a shows a greater surface temperature warming compared to air temperature for a cropland site. Contrarily to the short vegetation site, the warming rates of the two temperatures are similar for a forest site (Figure 1b). This indicates the strong aerodynamic coupling of diurnal air and surface temperatures in forests compared to short vegetation.

Certainly, it is intriguing to find out how evaporative conditions alter this coupling. In our earlier work (Panwar et al., 2019) we looked at the temperature warming rate for a cropland site in the Southern Great Plains (which is shown in Figure 1a). We observed that the warming rate of surface temperature decreases from dry (less-evaporative, sensible heat flux dominates) to moist (evaporative, latent heat

flux dominates) conditions but the warming rate of air temperature remained unaffected. Combining the boundary layer information and heat budget expression we explained that the diurnal variation of air temperature does not contain the imprints of evaporative conditions due to the compensating role of boundary layer development. If this is a general finding, then the surface temperature warming rate can be used for estimating evaporative conditions of short vegetation. Furthermore, it is also interesting to see how evaporative cooling competes with the cooling effect of a higher aerodynamic conductance of forests.

In this study, we approach two major questions to advance our understanding of diurnal temperature variations: a) Do the diurnal variations of surface and air temperature respond to evaporative conditions? And b) what is the role of the aerodynamic conductance of vegetation in altering these responses? Our previous work (Panwar et al., 2019) shows the stronger imprints of evaporative conditions in diurnal surface temperature variations in a cropland site. Here we examine the generality of this finding in short vegetation. Additionally, to understand the role of aerodynamic conductance in modifying these imprints we analyze data from the taller and more complex vegetation like savanna and forests.

We first present a model based on the surface energy balance to provide an expression for the diurnal temperature variation and its response to changes in evaporative conditions and aerodynamic conductance (all variables used are summarized in Table A1). Previous studies (Mallick et al., 2013; Ronda et al., 2001; Steduto and Hsiao, 1998) show diurnal variations in aerodynamic conductance, which is also considered in our model. To evaluate our model, we used observations from 51 FLUXNET sites that include short vegetation, savanna and forests. Surface and air temperature warming rates and their response to evaporative conditions are quantified for each site.

The observational analysis is followed by a demonstration of our model performance that reproduces observed temperature warming rates and their response to evaporative conditions. Using our model, we analyze the factors shaping the diurnal range of surface temperature (DT_sR). For this, the diurnal temperature range is obtained by combining the warming rates with the information on solar radiation. We conclude the study by demonstrating the contribution of solar radiation, evaporative fraction, aerodynamic conductance, and its diurnal variation in shaping DT_sR, using our observational analysis and model.

2 Modeling temperature-warming rate

Surface and air temperatures possess a strong diurnal variation that is driven by the absorption of solar radiation. The amplitude of this variation is also affected by other components of the surface energy balance, among which the partitioning of turbulent heat fluxes into latent and sensible heat is important. Generally, the surface energy balance is written as

$$R_s = R_{l,net} + LE + H + G \ . \qquad\qquad\qquad \text{Eq. (1)}$$

Here, R_s is the absorbed solar radiation at the surface, $R_{l,net}$ is the net longwave radiation, LE is the latent heat flux (with L being the latent heat of vaporization and E the evaporation rate), H is the sensible heat flux and G is the ground heat flux. For simplification of the surface energy balance we linearize $R_{l,net}$ using the first order terms, such that $R_{l,net} = R_o + k_r (T_s - T_{ref})$. Here, R_o is the net radiation at a reference temperature T_{ref}. The second term, $k_r = 4\,\sigma\,T_{ref}^3$ is the linearization constant. Incorporating this simplification of $R_{l,net}$ in Eq. (1), the surface energy balance can be rearranged to yield an expression for T_s,

$$T_s = T_{ref} + \frac{R_s - R_o - LE - H - G}{k_r} \qquad\qquad \text{Eq. (2)}$$

The warming rate of surface temperature is obtained by taking the derivative of Eq. 2 with respect to absorbed solar radiation, R_s, such that

$$\frac{dT_s}{dR_s} = \frac{1}{k_r} - \frac{1}{k_r} \cdot \frac{d(H + LE)}{dR_s} \qquad\qquad \text{Eq. (3)}$$

Since, R_o and T_{ref} are assumed to be constants and do not vary diurnally with R_s, they disappear in Eq. (3). Additionally, it is assumed that the diurnal change in G in response to R_s is negligible ($dG/dR_s \sim 0$) compared to the other components of surface energy balance. This assumption is valid since we are considering vegetated sites for our study, although we are aware that for non-vegetated surfaces G can represent a noticeable share of absorbed solar radiation (Clothier et al., 1986; Kustas and Daughtry, 1990).

We describe the evaporative conditions by the evaporative fraction (f_e), the ratio of the latent heat flux (LE) to the total turbulent heat fluxes ($H + LE$). Given this, the term $H + LE$ in Eq. (3) can be written as $H/(1 - f_e)$, which yields

$$\frac{dT_s}{dR_s} = \frac{1}{k_r} - \frac{1}{k_r} \cdot \frac{1}{(1 - f_e)} \cdot \frac{dH}{dR_s} \qquad\qquad \text{Eq. (4)}$$

Furthermore, the sensible heat flux can be expressed in terms of the aerodynamic conductance as $H = c_p\,\rho\,g_a(T_s - T_a)$, where c_p=1005 J kg^{-1} K^{-1} is the specific heat capacity of air, $\rho = 1.23$ kg m^{-3} is air density, g_a is the aerodynamic conductance, and $T_s - T_a$ is difference between surface and air temperature.

To use Eq. (4) to estimate warming rates, information is needed on dH/dR_s. Typically, H increases linearly with R_s in the morning, so that the derivative dH/dR_s is constant. Thus, the instantaneous response of H to R_s is equivalent to the mean response, such that dH/dR_s can be expressed as

$$\frac{dH}{dR_s} = c_p . \rho . \left[\overline{(T_s - T_a)}.\frac{dg_a}{dR_s} + \overline{g_a} . \frac{d(T_s - T_a)}{dR_s} \right] \qquad \text{Eq. (5)}$$

Here, $\overline{(T_s - T_a)}$ and $\overline{g_a}$ are the morning to noon means of $T_s - T_a$ and g_a. The diurnal variations of g_a and $T_s - T_a$ are captured by the terms dg_a/dR_s and $d(T_s - T_a)/dR_s$. When including Eq. (5) in Eq. (4), we get an approximation for the surface temperature warming rate given by,

$$\frac{dT_s}{dR_s} = \frac{(1-f_e) - c_p.\rho.[\overline{(T_s - T_a)}.dg_a/dR_s - \overline{g_a} . (dT_a/dR_s)]}{k_r.(1-f_e) + c_p.\rho.\overline{g_a}} \qquad \text{Eq. (6)}$$

Here, dT_a/dR_s is the warming rate of air temperature. We can further simplify this expression by considering the two terms in the denominator of Eq. (6). Considering $T_{ref} \sim 288$ K, the term $k_r(1-f_e)$ varies between ~ 4.87 W m^{-2} K^{-1} and ~ 0.54 W m^{-2} K^{-1} from dry ($f_e=0$) to moist ($f_e=1$) conditions, which is much smaller in magnitude compared to the term $c_p.\rho.\overline{g_a}$ that is ~ 60 W m^{-2} K^{-1} for a typical cropland site ($\overline{g_a}=0.05$ m s^{-1}) and 250 W m^{-2} K^{-1} for a typical forest site ($\overline{g_a}=0.2$ m s^{-1}). Because of these magnitudes, the term $k_r(1-f_e)$ can be neglected. This leads to a further simplification of the warming rate to

$$\frac{dT_s}{dR_s} \approx \frac{(1-f_e)}{c_p . \rho . \overline{g_a}} + \frac{dT_a}{dR_s} - \frac{\overline{(T_s - T_a)}}{\overline{g_a}} . \frac{dg_a}{dR_s} \qquad \text{Eq. (7)}$$

Eq. (7) shows that the morning to noon warming rate of surface temperature is a function of evaporative fraction, the warming rate of air temperature, the mean difference of surface and air temperature, the mean aerodynamic conductance, and also the sensitivity of aerodynamic conductance to solar radiation. On multiplying Eq. (7) with daily maximum solar radiation shall provide an approximation of diurnal range of surface temperature (DT$_s$R)

$$DT_sR \approx \frac{(1-f_e)}{c_p . \rho . \overline{g_a}} . R_{s,max} + DT_aR - \frac{\overline{T_s - T_a}}{\overline{g_a}} . \frac{dg_a}{dR_s} . R_{s,max} \qquad \text{Eq. (8)}$$

The DT$_s$R approximation can be validated with the observational data. Using Eq. (8), the contribution of $f_e, \overline{g_a}$, and dg_a/dR_s in shaping DT_sR can be quantified.

Next, the sensitivity of the warming rate to changes in evaporative conditions is obtained by taking the derivative of Eq. (7) with respect to evaporative fraction (f_e). To express these derivatives with respect to evaporative fraction, we use the prime $(dx/df_e = (x)')$. Therefore, $(dT_s/dR_s)'$ and $(dT_a/dR_s)'$

represent the change in surface and air temperature warming rates due to a unit change in evaporative fraction. The sensitivity of the warming rate of surface temperature to evaporative fraction is

$$\left(\frac{dT_s}{dR_s}\right)' = -\frac{1}{c_p \cdot \rho \cdot \overline{g_a}} + \left(\frac{dT_a}{dR_s}\right)' - \left[\frac{\overline{(T_s - T_a)}}{\overline{g_a}} \cdot \frac{dg_a}{dR_s}\right]' \qquad \text{Eq. (9)}$$

Eq. (9) is a negative quantity provided $(dT_a/dR_s)'$ and the third term response to evaporative fraction are small (or negative). The negative sign means that the warming rate decreases with an increase in evaporative fraction. The amplitude of this decrease mainly depends on the mean aerodynamic conductance $(\overline{g_a})$ and also on its diurnal sensitivity to solar radiation (dg_a/dR_s).

We next look into observations to obtain the values in Eq. 7 to predict the warming rate of surface temperature: f_e, $\overline{g_a}$, $\overline{T_s - T_a}$, and dg_a/dR_s. Likewise, using Eq. (9) requires the observations to quantify the sensitivities of the components of its third term $(\overline{T_s - T_a}, 1/\overline{g_a},$ and $dg_a/dR_s)$ to evaporative fraction. We derive these quantities from observations to then show that Eq. 7 reproduces the warming rate of surface temperature and its sensitivity to evaporative fraction using Eq. (9). Lastly, using the values from observations and our model expression for DT_sR, shown in Eq. (8), we estimate the contribution of the evaporative fraction and aerodynamic properties in shaping the magnitude of the diurnal surface temperature range.

3 Data and method

We use observations from 51 FLUXNET sites representing different vegetation types. The FLUXNET data consists of sensible and latent heat fluxes using the standard eddy covariance method and provides half hourly radiation and meteorological data (Baldocchi et al., 2001). The selected 51 sites contain data of the surface energy balance components and temperatures for more than four years. To avoid the effect of energy limitation on evaporation, only summer days are considered. Summer is defined here as days having greater daily mean incoming solar radiation at the surface than the median of the annual distribution. This approach standardizes the definition of summer days for sites at different latitudes and provides the days with comparable solar energy input for the individual sites.

Furthermore, among summer days, only clear sky days are considered to avoid the influence of clouds on temperatures. A filter to remove cloudy days is applied that is based on the quantile regression method using surface solar radiation and potential solar radiation (Renner et al., 2019). This method was applied only from morning to noon, so that the day with clouds in the evening is also considered as a clear sky day. This does not influence warming rates since they are calculated only from the morning to noontime variation of temperature.
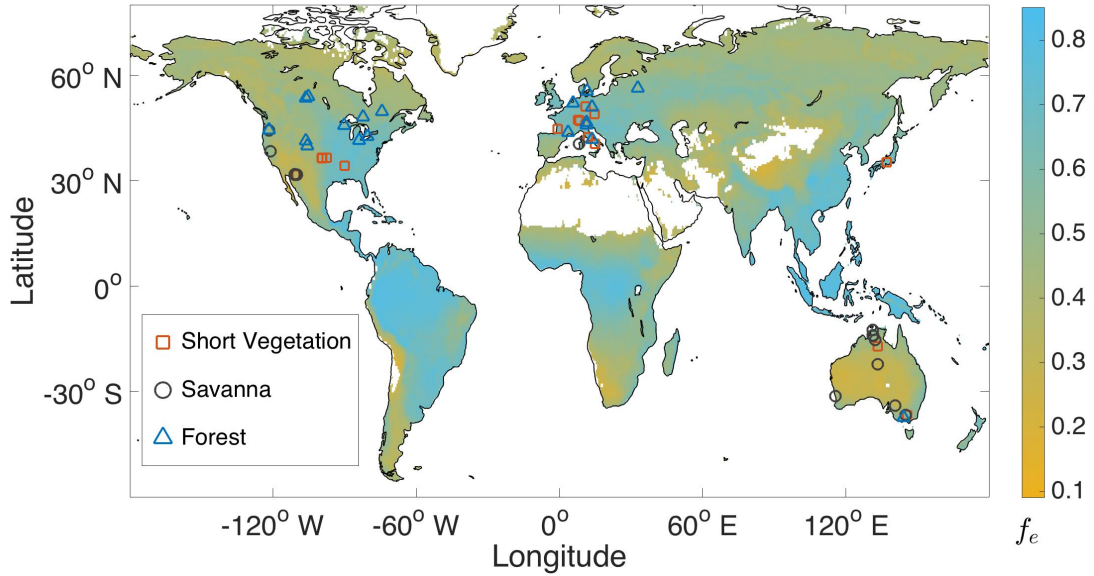
Figure 2 Geographical locations of FLUXNET sites used in this study. The vegetation type at each site is shown by the symbols. The color bar shows the mean annual evaporative fraction (f_e) derived from FLUXCOM data (year: 2001 to 2013).

The information on vegetation type is obtained from the FLUXNET land cover classification (Falge et al., 2017), which is based on the International Geosphere-Biosphere Programme (IGBP) Data and Information System. The IGBP land cover product is available at 1 km resolution and was derived from the Advance Very High Resolution Radiometer (Loveland and Belward, 1997). Detailed information of each site with their location, number of days used in the analysis, land cover type and references is provided in the Appendix (Table A2). Vegetation are classified into three types that is based on their typical height and coverage, see Table 1. Shorter vegetation like croplands, grasslands, and shrublands are grouped into the 'short vegetation' type. Savanna ecosystems are complex with heterogeneous vegetation height, which basically delineates the transition of short vegetation to forests, and are grouped into the 'savanna' type. All forest types, including deciduous broadleaf, evergreen broadleaf, evergreen needleleaf and mixed, are grouped in the 'forest' type.

The geographic location of the selected 51 sites is shown in Figure 2. The color bar represents the mean annual evaporative fraction derived from FLUXCOM data (Jung et al., 2019; Tramontana et al., 2016). Selected sites represent a wide range of ecosystems that is ideal for studying the generality of the response of warming rates to differences in evaporative conditions and vegetation type.

Table 1. Land cover types of the different sites considered here and their grouping into the short vegetation, savanna and forest types.

Vegetation types	Land use type	Number of sites
Short Vegetation	Cropland	12

	Grassland	6
	Shrubland	5
Savanna	Savanna	4
	Woody Savanna	5
Forest	Deciduous broadleaf forest	4
	Evergreen broadleaf forest	1
	Evergreen needle leaf forest	9
	Mixed forest	5

Evaporative conditions are quantified by evaporative fraction. One of the advantages of the evaporative fraction is its stability for daylight hours such that it can be assumed to be constant over a day (Shuttleworth et al., 1989). The daily mean evaporative fraction is obtained by the linear regression of half hourly morning to noon values of latent heat flux to the total turbulent heat fluxes. Similarly, a linear regression of daily mean warming rates and daily mean evaporative fractions is used to quantify the sensitivity of the warming rate to evaporative fraction.

We use the term air temperature for the temperature measured above the canopy, which is typically at 2 meters height. Surface temperature is calculated from the upwelling flux of longwave radiation using the Stefan-Boltzmann law, such that it represents the skin temperature of the vegetated surface. The aerodynamic conductance (g_a) is obtained from the observed sensible heat flux from $g_a = H/ (c_p . \rho . (T_s - T_a))$. Since aerodynamic conductance is not constant over the day, its diurnal variation is described by dg_a/dR_s, which is estimated from a linear regression of morning to noon half hourly values of g_a and R_s.

4 Results

4.1 Observational analysis

The primary advantage of the warming rate over DTR is its suitability to compare sites with different solar energy input. This is apparent from Figure 3, where we show the density distribution of the observed daily warming rates of (a) surface and (b) air temperatures for short vegetation, savanna, and forest. The warming rates of surface temperature for short vegetation, with a median value of 31.42 x 10^{-3} K (W m^{-2})$^{-1}$ are larger by almost a factor of two compared to the respective warming rates of forests with a median value of 15.47 x 10^{-3} K (W m^{-2})$^{-1}$. Savanna covers the range in warming rates of surface temperature with a median value of 27.09 x 10^{-3} K (W m^{-2})$^{-1}$, reflecting their characteristics being positioned between short vegetation and forests. Hence, the warming rates of surface temperature clearly show similar characteristics across different sites as well as a clear influence of vegetation type.

Surprisingly, this is not true for the warming rates of air temperature. All vegetation types show very similar distributions (Figure 3b). For short vegetation, this distribution is markedly shifted to smaller values, with a median of 12.32 x 10^{-3} K (W m^{-2})$^{-1}$, than the respective distribution for the warming rates

of surface temperature. Conversely, in forests, the distributions are similar (with a median of 11.13 x 10^{-3} K (W m^{-2})$^{-1}$), indicating the strong aerodynamic coupling between surface and air temperatures. The distribution for savanna has a median of 14.43 x 10^{-3} K (W m^{-2})$^{-1}$.
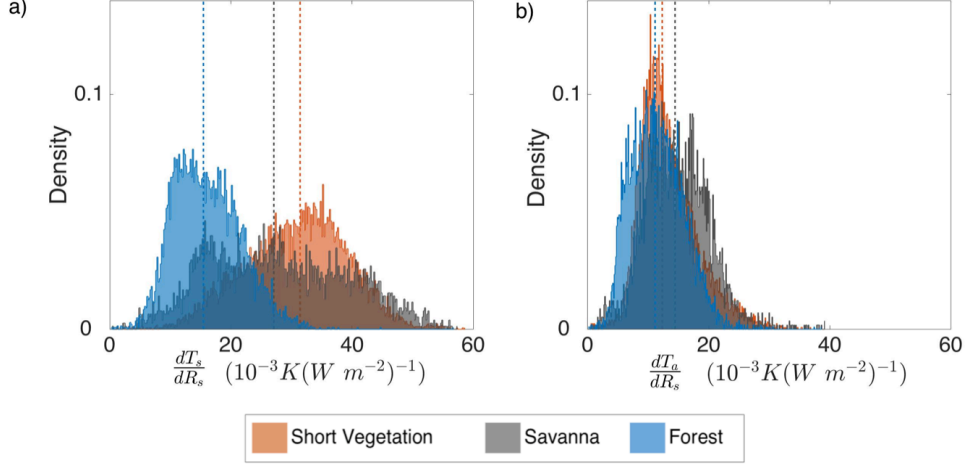
Figure 3 Density distribution of observed warming rates of (a) surface temperature and (b) air temperature for short vegetation, savanna, and forest. The vertical dashed lines indicate the median of each distribution in the respective colors of the vegetation types.

Within the short vegetation type, grassland and shrubland sites show much greater warming rates of surface temperature than cropland sites (Site-specific information on warming rates is provided in Figure A1 in the Appendix). This distinction could be attributed to site-specific evaporative conditions. Most of the shrubland sites are drier, while cropland sites are generally moister. Such an uneven distribution of evaporative conditions could impact the estimation of warming rates, such that it is higher for dry and lower for moist sites. On the other hand, despite these differences in the mean evaporative conditions, the sites contain days with a good range of evaporative fractions (see Figure A2 in Appendix). The range of evaporative fractions is important for the estimation of the sensitivity of the warming rates to evaporative fraction.

Next, we quantify the sensitivity of warming rates to evaporative fraction, $(dT/dR_s)'$, from the linear regression of the daily means. The value of this sensitivity represents the change in warming rate from dry (f_e=0) to moist (f_e=1) conditions, although we should note that these extreme values for the evaporative fraction are hypothetical. Figure 4 shows the mean sensitivity of the warming rates of surface (orange) and air (blue) temperature to evaporative fraction for short vegetation, savanna and forest (for site-specific responses, see Figure A2 in the Appendix). The sensitivity for short vegetation shows a strong decrease of ~23 x 10^{-3} K (W m^{-2})$^{-1}$ for surface temperature, but a much smaller decrease by ~5 x 10^{-3} K (W m^{-2})$^{-1}$ for air temperature. In our earlier work, similar responses were found for a cropland site (Figure A2, site no. 8). The savanna vegetation type shows a weaker decrease of ~12 x 10^{-3} K (W m^{-2})$^{-1}$ for surface temperature, but the warming rate of air temperature is almost insensitive

to evaporative fraction. In forests, both warming rates show very weak to almost no sensitivity to evaporative fraction.
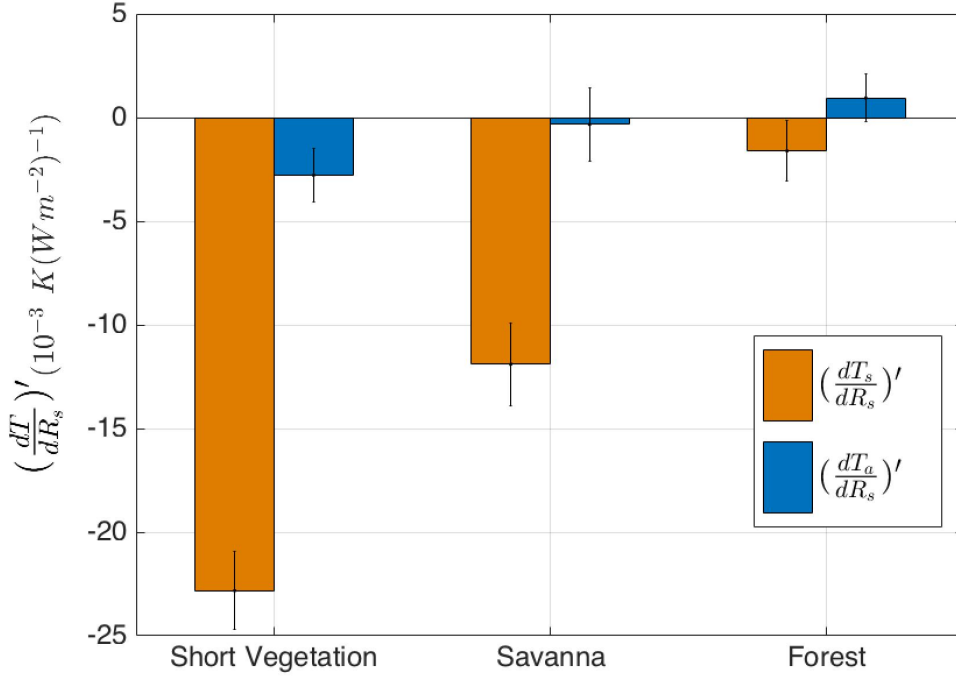
Figure 4 Bar plot of the sensitivity of warming rates of surface $(dT_s/dR_s)'$, and air $(dT_a/dR_s)'$ temperatures to evaporative fraction from observations for short vegetation, savanna, and forests. The error bars represent the standard error of the mean.

In addition to evaporative fraction, the aerodynamic conductance also influences the diurnal variation of temperatures. The aerodynamic conductance governs the ventilation of energy and mass from the surface to the atmosphere (Thom, 1972). Figure 5a shows the density distribution of morning to noon mean of aerodynamic conductance for the short vegetation, savanna, and forest sites. The mean aerodynamic conductance is usually a characteristic of vegetation height (Jones, 1992). We find that the aerodynamic conductance of short vegetation is much lower (median=0.022 m s^{-1}) than for forest (median=0.32 m s^{-1}). Savanna sites have similar aerodynamic conductance (median=0.023 m s^{-1}) as short vegetation but some woody savanna sites show relatively higher aerodynamic conductance (as shown by the second peak around 0.08 m s^{-1} in the distribution in Figure 5a).

Aerodynamic conductance typically increases substantially during the day, increasing roughly linearly with absorbed solar radiation, which is captured by dg_a/dR_s (Figure 5b). The positive sign of dg_a/dR_s reflects the increase in g_a from morning to noon, which is found for all vegetation types. Forest sites show a stronger increase, but note that these sites also have higher mean aerodynamic conductance. Overall, the aerodynamic conductance at noon is ~2.5 times the mean value across all vegetation types (calculated with a R$_{s,max}$=1000 W m^{-2}), indicating similar relative diurnal variations (see Table 2). In other words, the relative sensitivity of aerodynamic conductance, $1/\overline{g_a} \cdot dg_a/dR_s \approx$

$2.5 \times 10^{-3}(\text{W m}^{-2})^{-1}$ is about the same across the different sites. Because a greater aerodynamic conductance is expected to cool the surface more effectively, we expect that the diurnal increase in aerodynamic conductance shall reduce the warming rates of surface temperature (which can also be seen in Eq. 7, where the last term on the right-hand side is negative). Thus, in addition to the mean aerodynamic conductance, its diurnal variation is another important factor, which shapes the diurnal variation of temperatures.
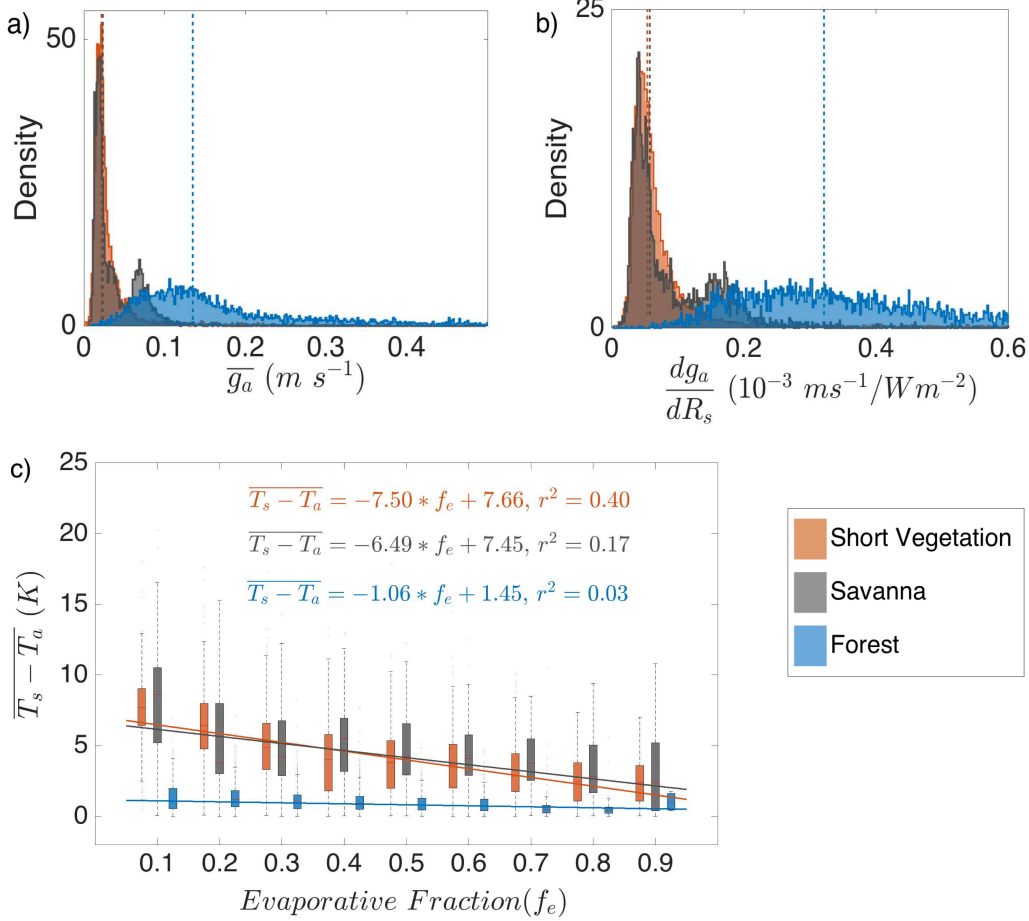
Figure 5 Density distributions inferred from observations of the morning to noon (a) mean aerodynamic conductance ($\overline{g_a}$), and (b) its sensitivity to solar radiation (dg_a/dR_s). The vertical dashed lines show the medians of the distributions. Also shown in (c) is the sensitivity of the morning to noon mean surface and air temperature difference ($\overline{T_s - T_a}$) to evaporative fraction, which is a sensitivity needed for the estimation of how the warming rate of surface temperature responds to evaporative fraction using Eq. (9). The bars indicate the 25th and 75th percentiles of the observations, respectively. The lines are the best fit for the linear regression of $\overline{T_s - T_a}$ and evaporative fraction for each vegetation type, with the equations and r^2 shown in the plot.

Table 2 First quartile (Q1), median, and third quartile (Q3) for the distributions of dT_s/dR_s, dT_a/dR_s, $\overline{g_a}$, and dg_a/dR_s for short vegetation, savanna and forest.

Vegetation	dT_s/dR_s	dT_a/dR_s	$\overline{g_a}$	dg_a/dR_s

		$(10^{-3}\,K\,(W\,m^{-2})^{-1})$	$(10^{-3}\,K\,(W\,m^{-2})^{-1})$	$(m\,s^{-1})$	$(10^{-3}\,m\,s^{-1}\,/W\,m^{-2})$
Short Vegetation	Q1	25.1	9.9	0.017	0.041
	Median	31.4	12.3	0.022	0.054
	Q3	36.7	15.7	0.032	0.078
Savanna	Q1	18.6	10.9	0.037	0.040
	Median	27.1	14.4	0.023	0.058
	Q3	36.8	18.1	0.060	0.137
Forest	Q1	11.8	8.1	0.093	0.229
	Median	15.5	11.1	0.135	0.321
	Q3	19.7	14.3	0.204	0.444

To estimate the warming rate of surface temperature and its sensitivity to evaporative fraction using Eqns. 7 – 9, we also need to know the mean difference of surface and air temperature $(\overline{T_s - T_a})$. We find that $\overline{T_s - T_a}$ is higher in short vegetation and savanna compared to forest sites. Additionally, $\overline{T_s - T_a}$ decreases on days with high evaporative fraction in short vegetation and savanna, but not in forests. Betts and Ball (1995) showed a similar sensitivity of $\overline{T_s - T_a}$ to evaporative conditions in a grassland site. Unlike $\overline{T_s - T_a}$, we found no such sensitivity of $\overline{g_a}$ and dg_a/dR_s to evaporative fraction. This finding is different to the study by Rigden and Li (2017) who showed that the aerodynamic resistance depends on the Bowen ratio. This difference can be attributed to their way to estimate aerodynamic resistance from the frictional velocity and wind speeds, which assumes neutral conditions, whereas we obtain aerodynamic conductance from sensible heat flux.

Given that only the mean temperature difference, $\overline{T_s - T_a}$, is sensitive to evaporative fraction while $\overline{g_a}$ and dg_a/dR_s are not, the last term in Eq. (9) reduces to the sensitivity of this temperature difference to evaporative fraction. This sensitivity is shown in Figure 5c. The third term of Eq. (9) thus depends mostly on $(\overline{T_s - T_a})'$ because the relative diurnal variation of aerodynamic conductance $(1/\overline{g_a} \cdot dg_a/dR_s)$ is similar for all vegetation types.

To summarize our analysis of observations, we found that the diurnal variation of surface temperature of short vegetation showed much stronger imprints of evaporative conditions than air temperature. In forests, the diurnal variations of both, surface and air temperature, were found to be insensitive to evaporative conditions. The mean aerodynamic conductance derived from observations confirm the characteristic high values for forests compared to short vegetation. Additionally, we found a strong diurnal variation of the aerodynamic conductance that in relative terms is comparable for all vegetation types.

To explain these findings, we hypothesize that the high aerodynamic conductance of forests lowers the diurnal increase in surface temperature, as it provides greater ventilation. Since air temperatures do not respond to evaporative fraction, we therefore expect the warming rate of surface temperature of forests

to be less sensitive. This can already be anticipated from Eq. 9, together with the values provided in Table 2 and the sensitivities shown in Figure 5c. Using these values, Eq. 9 yields an estimate for the sensitivity of the warming rate of surface temperature to evaporative fraction for short vegetation of about -24×10^{-3} K (W m^{-2})$^{-1}$ and -4×10^{-3} K (W m^{-2})$^{-1}$ for forests, similar to what is shown in Figure 4. In the following, we verify our model expression in greater detail.

4.2 Model application and interpretation

To estimate the warming rate of surface temperature using Eq. (7) in greater detail, we used daily values of observed f_e, $\overline{g_a}$, dT_a/dR_s, $\overline{T_s - T_a}$, and dg_a/dR_s. Since dT_a/dR_s is similar for all sites, the diurnal variation of air temperature does not seem to depend on the diurnal variation of surface temperature, and vice versa. Figure 6 a shows the comparison of the modeled warming rates to those derived from observations. The model performs very well for all sites for the given information, with coefficients of determination (r^2) of $r^2 = 0.69$ for short vegetation, $r^2 = 0.87$ for savanna, and $r^2 = 0.53$ for forests. Similarly, the slopes (m) of the regression between modeled and observed dT_s/dR_s are close to 1 for short vegetation (m = 0.85) and savanna (m = 0.90), meaning the dT_s/dR_s magnitudes are well captured by our model, although the slope is too low for forests (m = 0.77). However, at some sites with short vegetation, dT_s/dR_s is underestimated. We speculate that these are the sites with non-vegetated surfaces where the ground heat flux contribution to diurnal surface temperature variations can be significant (Saltzman and Pollack, 1977) which is currently neglected in our model.

It is apparent from Figure 6 a, that the warming rates for surface temperature are higher for short vegetation compared to that of forests. This is mainly due to the relatively high aerodynamic conductance of forest, which reduces the magnitude of the first and third term on the right-hand side of Eq. 7.

The greater aerodynamic conductance of forests also reduces the sensitivity of warming rates to evaporative fraction compared to short vegetation, which can be seen in Eq. (9). Note that the diurnal variation of the aerodynamic conductance is included here by the term dg_a/dR_s in our estimates. Eq. (9) reproduces the response of the warming rates to evaporative fraction quite well for all vegetation types (m= 0.88, $r^2 = 0.45$, Figure 6 b), including their ranges. Certain deviations exist because there are some biases in the number of moist and dry days in the observations that are reflected in the horizontal error bars. The other possible cause for bias is the large variation in the sensitivity of $\overline{T_s - T_a}$ to f_e in short vegetation and savanna (Figure 5c).
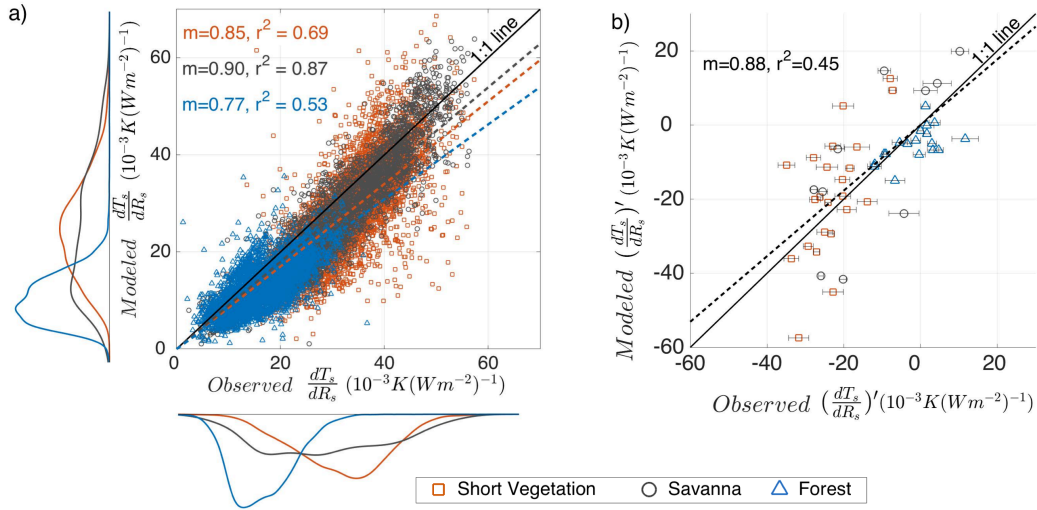
Figure 6 a) Modeled versus observed warming rates, dT_s/dR_s for each site, for the three vegetation types. The density distributions show the spread. The coefficient of determination (r^2) and slope (m) of the linear fit (dashed lines) are depicted for each vegetation type. b) Model evaluation of the sensitivity of the warming rates to evaporative fraction, $(dT_s/dR_s)'$, with those derived from observations for each site.

We next link our estimates for warming rates back to the diurnal surface temperature range (DT_sR) by multiplying the expression for the warming rate with the daily maximum of absorbed solar radiation, $R_{s,max}$ (see Eq. 8). To understand how solar radiation, evaporative fraction, and the mean aerodynamic conductance, and its diurnal variation contribute to DT_sR separately, we consider four cases. In first case, we assume that the diurnal variation in surface temperature is solely driven by solar radiation, such that there is no evaporation ($f_e = 0$) and the surface has a low and constant aerodynamic conductance of $g_a = 0.022$ m s^{-1}, which is the median of the aerodynamic conductance of short vegetation (see Table 2). Figure 7 a shows that in this case, DT_sR is overestimated for all vegetation types (regression slope m > 1) with a low $r^2 \leq 0.3$. This greater warming indicates that vegetation and evaporation cools surface temperatures and reduces the diurnal surface temperature range.

In second case, we add the information on evaporative fraction (Figure 7 b). The DT_sR estimates for short vegetation (m=1.26, r^2=0.55) and to some extent for savanna (m=1.37, r^2=0.46) are considerably improved, but not for forests (m=2.22, r^2=0.18). Nevertheless, in this case, DT_sR is cooler and closer to the observed values than the previous case, indicating the importance of evaporation in cooling the diurnal temperature, although the values are still being too high, as indicated by the regression slopes being m > 1.

However, in forests, the information on evaporative fraction alone does not reduce DT_sR, because their high aerodynamic conductance is not accounted for. Therefore, in third case, in addition to absorbed solar radiation and evaporative fraction, we added the information on the mean aerodynamic

conductance ($\overline{g_a}$). The DT$_s$R in forests is now better captured ($r^2 = 0.35$) and the magnitude is closer to the observed (m=0.98), see Figure 7c. In short vegetation and savanna, however, DT$_s$R is still mostly overestimated. This can be attributed to the diurnal variation of the aerodynamic conductance, dg_a/dR_s, not being included in this case.

Finally, we add information on all components to our estimate (Figure 7d). DT$_s$R estimates are much closer to the observation with a good r^2 for all vegetation types and regression slopes are reduced to values m < 1, indicating a slight cold bias. Forest sites show a slight improvement in r^2 although the contribution of dg_a/dR_s is comparatively small because $\overline{T_s - T_a}$ in the forest is small (~1 K).
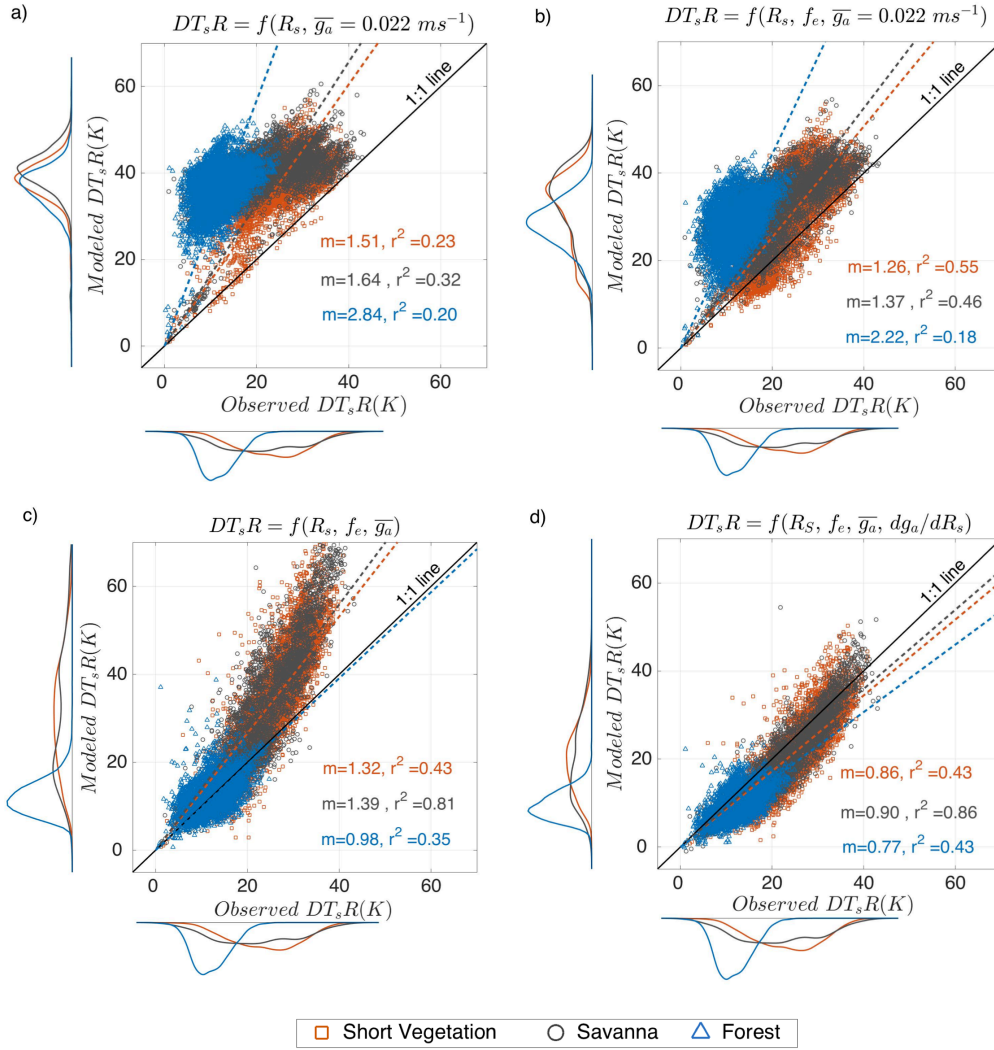
Figure 7 Comparison of the estimated diurnal surface temperature range (DT$_s$R) for short vegetation (red), savanna (grey) and forests (blue) with observations for four scenarios: a) DT$_s$R is only a function of solar radiation (R_s), b) DT$_s$R including the effect of evaporative fraction (f_e), c) DT$_s$R with the additional effect of differences in mean aerodynamic conductance between vegetation types ($\overline{g_a}$), and d) DT$_s$R additionally includes the effect of the diurnal variation in aerodynamic conductance,

(dg_a/dR_s). Dashed lines show the linear regression between model and observation with their slopes (m) and coefficient of determination indicated (r^2) in the plots.

These four cases show that vegetation type and evaporative conditions play significant roles in modulating the diurnal variation in surface temperature. Evaporative fraction is important to reduce the spread and magnitude (as indicated by the lower values of m and higher r^2) whereas differences in the mean aerodynamic conductance are important to capture the different magnitudes of DT_sR between short vegetation and forests.

The importance of these factors can be illustrated by how much they act to reduce the magnitude of DT_sR. This can be done by evaluating the extent to which the regression slope, m, is reduced by these factors, using the first case that only considers solar radiation as the reference case. Evaporation reduces DT_sR by ~18 % (short vegetation: (1.26-1.51)/1.51 = -16.55 %, savanna: (1.37 – 1.64)/1.64 = -16.46 %, and forest: (2.22 – 2.84)/2.84 = -21.83 %). On comparing Figure 7 b and 7c, we found that the high aerodynamic conductance of forests reduces DT_sR by 56 % ((0.98 – 2.22)/2.22 = -56%). In other words, the higher aerodynamic conductance of forests causes a substantially larger cooling than evaporation. The diurnal variation of the aerodynamic conductance then reduces the DT_sR further, being stronger in short vegetation ((0.86 – 1.32)/1.32 = -35%) and savanna ((0.90 – 1.40)/1.75 = -35.25 %) than in forests ((0.77 – 0.98)/0.98= -21%).

5 Discussion

We demonstrate a robust way of characterizing the diurnal variation of temperatures using their morning to noon warming rates, which are derived from the half hourly changes in temperatures and absorbed solar radiation. Warming rates are suitable for the analysis of other factors that affect temperatures, such as evaporation and vegetation, because the most dominant variation in temperatures caused by solar energy input is removed.

Our analytic surface energy balance model can reproduce the warming rates of surface temperature derived from observations quite well and shows the physical significance of evaporative fraction, aerodynamic conductance and its diurnal variation in shaping diurnal temperature variations. The approximations made in the derivation of Eqns. 7 and 9 can further be improved by a more detailed formulation of net longwave radiation (which could, for instance, include optical properties of the atmosphere) and the ground heat flux. Warming rates may also likely to be sensitive to clouds and might not capture the information of evaporative conditions and vegetation on cloudy days. These effects were not evaluated here because we focused the analysis on clear sky days. It may, however, very well be that the dominant effect of clouds is simply to reduce absorbed solar radiation, so that Eqns. 7 and 9 could also predict warming rates for those conditions. Also, we did not provide a way to estimate warming rates of air temperature. These could be topics for future research.

One of the main findings of our study is the contrasting response of warming rates of surface and air temperature to evaporative fraction. The warming rate of air temperature does not contain any imprints of evaporative fraction across all sites, irrespective of their aerodynamic conductance and evaporative conditions. This finding is consistent with our previous work (Panwar et al., 2019), where we explained this finding by the effect of boundary layer growth that compensates the effects of different evaporative conditions. We anticipate that our hypothesis of the compensating effect of boundary layer growth might also hold for forests, but this would need further research.

The warming rate of surface temperature is strongly sensitive to evaporative fraction for short vegetation. The mean sensitivity of $\sim23 \times 10^{-3}$ K (W m^{-2})$^{-1}$ is consistent with the reported sensitivity in Panwar et al. (2019). This decrease is comparable for all sites with short vegetation and we anticipate that some of the spread is due to their somewhat different aerodynamic properties. Another source of uncertainty is the uneven distribution of days of different evaporative fractions, which may affect the estimation of the sensitivity. This uncertainty could be reduced by longer time series of observations to obtain a greater sampling range of evaporative conditions.

The notion that surface and air temperature variations respond differently to evaporative conditions was reported in previous research (Cresswell et al., 1999; Fu et al., 2011; Hengl et al., 2012; Jang et al., 2004; Kilibarda et al., 2014; Zhu et al., 2013) and is relevant when air temperature products are developed from remotely sensed surface temperature. Typically, these products are primarily based on the assumption that surface temperature is a proxy of air temperature. Generally, these approaches overestimate daytime air temperature (Oyler et al., 2016; Zhang et al., 2011). This is consistent with our analysis, which shows markedly higher warming rates of surface temperature for non-forested vegetation than the warming rates of air temperature (see Figure 3). This overestimate can also be understood by the first term on the right-hand side of Eq. 7, which causes the stronger response of surface temperature compared to air temperature to changes in absorbed solar radiation.

Our study shows that the warming rates of surface and air temperature are similar at forest sites, which indicates the strong coupling between the two temperatures. This finding is in agreement with the previous study by Li et al., 2015 and Mildrexler et al., 2011, where evaporative cooling and the high aerodynamic conductance of forests were identified as the responsible factors for the strong coupling between surface and air temperature. Additionally, we show that the diurnal variation of surface and air temperature remains similar irrespective of the evaporative conditions in the forest. We can only speculate about the physical mechanism behind this finding. While it is well established that the greater aerodynamic roughness of the forest leads to a greater aerodynamic conductance for neutral conditions (T.R. Oke, 2002) we also find that the diurnal variation is much larger than the mean (the term dg_a/dR_s). This enhancement is most likely related to buoyancy, which is produced when the surface is heated by the absorption of solar radiation during the day. The finding that the relative enhancement of aerodynamic conductance between forests and non-forests is the same, and that this enhancement is insensitive to evaporative fraction, seems to be surprising and would need further

investigations about their physical explanations.

We then applied our analytical model to estimate the diurnal surface temperature range DT_sR and attributed the dominant factors that influence this range. It attributed the low DT_sR of forests mostly to their high aerodynamic conductance (~56 %), with evaporation playing only a secondary role (~22 %). This finding is consistent with studies that showed that the warming induced by deforestation to be mainly the consequence of changes in aerodynamic conductance rather than changes in evaporative conditions (Bright et al., 2017; Chen and Dirmeyer, 2016; Lee et al., 2011b; Zhao et al., 2014b). This aerodynamic effect is thus important for the cooling effect of forests (Ellison et al., 2017; Li et al., 2015; Tang et al., 2018), which our analysis and analytical model supports.

In addition to the role of the mean aerodynamic conductance, we find a strong diurnal variation of the aerodynamic conductance that is greater than the mean (as already reported by Mallick et al., 2013; Ronda et al., 2001; Steduto and Hsiao, 1998). This diurnal variation acts to reduce the diurnal variation in surface temperature further. While our findings show that the relative diurnal variation in aerodynamic conductance is about the same across the sites, this variation caused a stronger reduction in DT_sR (~ -35 %) in short vegetation and savanna compared to forests (~ -21%). It indicates that in forests, the greater mean aerodynamic conductance is much more important than its diurnal variation. This can be explained by $\overline{T_s - T_a}$ being small (~1 K) in forests, although the reason for this small difference would need further evaluation.

Our model demonstrates a similar sensitivity of DT_sR to energy partitioning and aerodynamic conductance as a previous study by Diak and Whipple (1993), who used simulations with a boundary layer model. Our model can capture this sensitivity solely with surface energy balance information, but does not require information of the boundary layer (which is likely to be encapsulated in the warming rate of air temperature and its lack of sensitivity to evaporative fraction). This indicates that the diurnal variation in surface temperature is dominantly governed by the exchange at the surface, particularly regarding its aerodynamic conductance and the evaporative fraction.

To sum up this discussion, our findings are consistent with previously published research regarding the main factors that shape the diurnal variation of surface and air temperature across different vegetation types. The derived equations of the warming rate of surface temperature (Eq. 7) and its sensitivity to evaporative fraction (Eq. 9) appear to be useful to describe and quantify the primary factors that cause differences in the diurnal variation of surface temperature across different land cover types.

6 Conclusions

We used warming rates, the change in temperatures with a change in absorbed solar radiation from morning to solar noon, to identify the influences of evaporative conditions, and vegetation on diurnal temperature variations across 51 FLUXNET sites covering different vegetation types. We found that

the warming rates of air temperature are similar across the sites and are insensitive to evaporative fraction. The warming rates of surface temperatures of sites with short vegetation decreased with greater evaporative fraction, representing a stronger evaporative cooling. For forests, warming rates of surface temperature are almost the same as for air temperature and lacked sensitivity to evaporative fraction. Using an analytical description of the surface energy balance, we reproduced these findings and attributed the different response of forests primarily to their higher aerodynamic conductance.

From our analysis, we can draw several conclusions: First, we found that diurnal variations in air temperature reflect very little information of evaporative conditions, implying that these observations cannot be used to infer evaporation. Second, the diurnal variation of surface temperature, however, shows a clear sensitivity to evaporative fraction for short vegetation, so that evaporation may be inferred from surface temperature observations. Third, in forests, surface temperature is strongly aerodynamically coupled to air temperatures by their high aerodynamic conductance, so that these lack sensitivity to evaporative fraction. Hence, diurnal temperature variations of forested sites do not seem to carry a notable effect of evaporation. What this shows is that the effect of evaporative conditions on diurnal temperature variations delicately depends on the presence or absence of forests.

Data availability: For the map of evaporative fraction, we used the FLUXCOM monthly data of sensible and latent heat fluxes, available at http://www.fluxcom.org/. The observational analysis used FLUXNET data from 51 sites, available at https://fluxnet.fluxdata.org/. More description of each site is provided in the Appendix.

Author contribution: All authors conceived the study. AP analysed data, AK derived the energy-balance model that is further developed by AP. MR provided classification of cloud-free conditions. All authors interpreted results. AP wrote the manuscript with input of MR and AK.

Competing interests: The authors declare that they have no conflict of interest.

Acknowledgements: Annu Panwar shows her sincere thanks for the stipend from the International Max Planck Research School for Global Biogeochemical Cycles (IMPRS-gBGC) for performing this research.

References

Anderson, M. C., Allen, R. G., Morse, A. and Kustas, W. P.: Use of Landsat thermal imagery in monitoring evapotranspiration and managing water resources, Remote Sensing of Environment, 122, 50–65, doi:10.1016/j.rse.2011.08.025, 2012.

Baier, W. and Robertson, Geo. W.: Estimation of latent evaporation from simple weather observations, Can. J. Plant Sci., 45(3), 276–284, doi:10.4141/cjps65-051, 1965.

Baldocchi, D., Falge, E., Gu, L., Olson, R., Hollinger, D., Running, S., Anthoni, P., Bernhofer, C., Davis, K., Evans, R., Fuentes, J., Goldstein, A., Katul, G., Law, B., Lee, X., Malhi, Y., Meyers, T., Munger, W., Oechel, W., Paw, K. T., Pilegaard, K., Schmid, H. P., Valentini, R., Verma, S., Vesala, T.,

Wilson, K. and Wofsy, S.: FLUXNET: A New Tool to Study the Temporal and Spatial Variability of Ecosystem–Scale Carbon Dioxide, Water Vapor, and Energy Flux Densities, Bulletin of the American Meteorological Society, 82(11), 2415–2434, doi:10.1175/1520-0477(2001)082<2415:FANTTS>2.3.CO;2, 2001.

Betts, A. K. and Ball, J. H.: The FIFE surface diurnal cycle climate, Journal of Geophysical Research, 100(D12), 25679, doi:10.1029/94JD03121, 1995.

Bevan, S. L., Los, S. O. and North, P. R. J.: Response of vegetation to the 2003 European drought was mitigated by height, Biogeosciences, 11(11), 2897–2908, doi:10.5194/bg-11-2897-2014, 2014.

Blaney, H. F. and Cridlle, W. D.: Blaney HF, Criddle WD. 1950. Determining Water Requirements in Irrigated Areas from Climatological Irrigation Data. Technical Paper No. 96, US Department of Agriculture, Soil Conservation Service, Washington, D.C., 48 pp, , 48 pp, 1950.

Boegh, E., Soegaard, H. and Thomsen, A.: Evaluating evapotranspiration rates and surface conditions using Landsat TM to estimate atmospheric resistance and surface resistance, Remote Sensing of Environment, 79(2–3), 329–343, doi:10.1016/S0034-4257(01)00283-8, 2002.

Bright, R. M., Davin, E., O'Halloran, T., Pongratz, J., Zhao, K. and Cescatti, A.: Local temperature response to land cover and management change driven by non-radiative processes, Nature Clim Change, 7(4), 296–302, doi:10.1038/nclimate3250, 2017.

Bristow, K. L. and Campbell, G. S.: On the relationship between incoming solar radiation and daily maximum and minimum temperature, Agricultural and Forest Meteorology, 31(2), 159–166, doi:10.1016/0168-1923(84)90017-0, 1984.

Chen, L. and Dirmeyer, P. A.: Adapting observationally based metrics of biogeophysical feedbacks from land cover/land use change to climate modeling, Environ. Res. Lett., 11(3), 034002, doi:10.1088/1748-9326/11/3/034002, 2016.

Clothier, B. E., Clawson, K. L., Pinter, P. J., Moran, M. S., Reginato, R. J. and Jackson, R. D.: Estimation of soil heat flux from net radiation during the growth of alfalfa, Agricultural and Forest Meteorology, 37(4), 319–329, doi:10.1016/0168-1923(86)90069-9, 1986.

Cresswell, M. P., Morse, A. P., Thomson, M. C. and Connor, S. J.: Estimating surface air temperatures, from Meteosat land surface temperatures, using an empirical solar zenith angle model, International Journal of Remote Sensing, 20(6), 1125–1132, doi:10.1080/014311699212885, 1999.

Dai, A., Trenberth, K. E. and Karl, T. R.: Effects of Clouds, Soil Moisture, Precipitation, and Water Vapor on Diurnal Temperature Range, Journal of climate, 12, 23, 1999.

Diak, G. R. and Whipple, M. S.: Improvements to models and methods for evaluating the land-surface energy balance and 'effective' roughness using radiosonde reports and satellite-measured 'skin' temperature data, Agricultural and Forest Meteorology, 63(3–4), 189–218, doi:10.1016/0168-1923(93)90060-U, 1993.

Ellison, D., Morris, C. E., Locatelli, B., Sheil, D., Cohen, J., Murdiyarso, D., Gutierrez, V., Noordwijk, M. van, Creed, I. F., Pokorny, J., Gaveau, D., Spracklen, D. V., Tobella, A. B., Ilstedt, U., Teuling, A. J., Gebrehiwot, S. G., Sands, D. C., Muys, B., Verbist, B., Springgay, E., Sugandi, Y. and Sullivan, C. A.: Trees, forests and water: Cool insights for a hot world, Global Environmental Change, 43, 51–61, doi:10.1016/j.gloenvcha.2017.01.002, 2017.

Falge, E., Aubinet, M., Bakwin, P. S., Baldocchi, D., Berbigier, P., Bernhofer, C., Black, T. A., Ceulemans, R., Davis, K. J., Dolman, A. J., Goldstein, A., Goulden, M. L., Granier, A., Hollinger, D. Y., Jarvis, P. G., Jensen, N., Pilegaard, K., Katul, G., Kyawthapaw, P., Law, B. E., Lindroth, A., Loustau, D., Mahli, Y., Monson, R., Moncrieff, P., Moors, E., Munger, J. W., Meyers, T., Oechel, W., Schulze, E.-D., Thorgeirsson, H., Tenhunen, J., Valentini, R., Verma, S. B., Vesala, T. and Wofsy, S. C.: FLUXNET Research Network Site Characteristics, Investigators, and Bibliography, 2016, , 1459.4803539999996 MB, doi:10.3334/ORNLDAAC/1530, 2017.

Fu, G., Shen, Z., Zhang, X., Shi, P., Zhang, Y. and Wu, J.: Estimating air temperature of an alpine meadow on the Northern Tibetan Plateau using MODIS land surface temperature, Acta Ecologica Sinica, 31(1), 8–13, doi:10.1016/j.chnaes.2010.11.002, 2011.

Gallo, K. P.: The Influence of Land Use/Land Cover on Climatological Values of the Diurnal Temperature Range, JOURNAL OF CLIMATE, 9, 2941–2944, 1996.

Hargreaves, G. H. and Samani, Z. A.: Reference Crop Evapotranspiration from Temperature, Applied Engineering in Agriculture, 1(2), 96–99, doi:10.13031/2013.26773, 1985.

Hengl, T., Heuvelink, G. B. M., Perčec Tadić, M. and Pebesma, E. J.: Spatio-temporal prediction of daily temperatures using time-series of MODIS LST images, Theor Appl Climatol, 107(1–2), 265–277, doi:10.1007/s00704-011-0464-2, 2012.

Jackson, L. S. and Forster, P. M.: An Empirical Study of Geographic and Seasonal Variations in Diurnal Temperature Range, J. Climate, 23(12), 3205–3221, doi:10.1175/2010JCLI3215.1, 2010.

Jackson, T. J., Le Vine, D. M., Hsu, A. Y., Oldak, A., Starks, P. J., Swift, C. T., Isham, J. D. and Haken, M.: Soil moisture mapping at regional scales using microwave radiometry: the Southern Great Plains Hydrology Experiment, IEEE Transactions on Geoscience and Remote Sensing, 37(5), 2136–2151, doi:10.1109/36.789610, 1999.

Jang, J.-D., Viau, A. A. and Anctil, F.: Neural network estimation of air temperatures from AVHRR data, International Journal of Remote Sensing, 25(21), 4541–4554, doi:10.1080/01431160310001657533, 2004.

Jarvis, P. G. and Mcnaughton, K. G.: Stomatal Control of Transpiration: Scaling Up from Leaf' to Region, Advances in ecological research, 15, 49, 1986.

JONES, H. G.: Plants and Microclimate, p. 428 pp, Cambridge University Press., 1992.

Juang, J.-Y., Katul, G., Siqueira, M., Stoy, P. and Novick, K.: Separating the effects of albedo from eco-physiological changes on surface temperature along a successional chronosequence in the southeastern United States, Geophysical Research Letters, 34(21), doi:10.1029/2007GL031296, 2007.

Jung, M., Koirala, S., Weber, U., Ichii, K., Gans, F., Camps-Valls, G., Papale, D., Schwalm, C., Tramontana, G. and Reichstein, M.: The FLUXCOM ensemble of global land-atmosphere energy fluxes, Scientific Data, 6(1), doi:10.1038/s41597-019-0076-8, 2019.

Kilibarda, M., Hengl, T., Heuvelink, G. B. M., Gräler, B., Pebesma, E., Perčec Tadić, M. and Bajat, B.: Spatio-temporal interpolation of daily temperatures for global land areas at 1 km resolution, J. Geophys. Res. Atmos., 119(5), 2294–2313, doi:10.1002/2013JD020803, 2014.

Kustas, W. P. and Daughtry, C. S. T.: Estimation of the soil heat flux/net radiation ratio from spectral data, Agricultural and Forest Meteorology, 49(3), 205–223, doi:10.1016/0168-1923(90)90033-3, 1990.

Kustas, W. P. and Norman, J. M.: Evaluation of soil and vegetation heat flux predictions using a simple two-source model with radiometric temperatures for partial canopy cover, Agricultural and Forest Meteorology, 94(1), 13–29, doi:10.1016/S0168-1923(99)00005-2, 1999.

Lee, X., Goulden, M. L., Hollinger, D. Y., Barr, A., Black, T. A., Bohrer, G., Bracho, R., Drake, B., Goldstein, A., Gu, L., Katul, G., Kolb, T., Law, B. E., Margolis, H., Meyers, T., Monson, R., Munger, W., Oren, R., Paw U, K. T., Richardson, A. D., Schmid, H. P., Staebler, R., Wofsy, S. and Zhao, L.: Observed increase in local cooling effect of deforestation at higher latitudes, Nature, 479(7373), 384–387, doi:10.1038/nature10588, 2011a.

Lee, X., Goulden, M. L., Hollinger, D. Y., Barr, A., Black, T. A., Bohrer, G., Bracho, R., Drake, B., Goldstein, A., Gu, L., Katul, G., Kolb, T., Law, B. E., Margolis, H., Meyers, T., Monson, R., Munger, W., Oren, R., Paw U, K. T., Richardson, A. D., Schmid, H. P., Staebler, R., Wofsy, S. and Zhao, L.:

Observed increase in local cooling effect of deforestation at higher latitudes, Nature, 479(7373), 384–387, doi:10.1038/nature10588, 2011b.

Li, Y., Zhao, M., Motesharrei, S., Mu, Q., Kalnay, E. and Li, S.: Local cooling and warming effects of forests based on satellite observations, Nat Commun, 6(1), 6603, doi:10.1038/ncomms7603, 2015.

Lindvall, J. and Svensson, G.: The diurnal temperature range in the CMIP5 models, Clim Dyn, 44(1–2), 405–421, doi:10.1007/s00382-014-2144-2, 2015.

Liu, B., Xu, M., Henderson, M., Qi, Y. and Li, Y.: Taking China's Temperature: Daily Range, Warming Trends, and Regional Variations, 1955–2000, J. Climate, 17(22), 4453–4462, doi:10.1175/3230.1, 2004.

Loveland, T. R. and Belward, A. S.: The International Geosphere Biosphere Programme Data and Information System global land cover data set (DISCover), Acta Astronautica, 41(4–10), 681–689, doi:10.1016/S0094-5765(98)00050-2, 1997.

Luyssaert, S., Jammet, M., Stoy, P. C., Estel, S., Pongratz, J., Ceschia, E., Churkina, G., Don, A., Erb, K., Ferlicoq, M., Gielen, B., Grünwald, T., Houghton, R. A., Klumpp, K., Knohl, A., Kolb, T., Kuemmerle, T., Laurila, T., Lohila, A., Loustau, D., McGrath, M. J., Meyfroidt, P., Moors, E. J., Naudts, K., Novick, K., Otto, J., Pilegaard, K., Pio, C. A., Rambal, S., Rebmann, C., Ryder, J., Suyker, A. E., Varlagin, A., Wattenbach, M. and Dolman, A. J.: Land management and land-cover change have impacts of similar magnitude on surface temperature, Nature Climate Change, 4(5), 389–393, doi:10.1038/nclimate2196, 2014.

Makowski, K., Jaeger, E. B., Chiacchio, M., Wild, M., Ewen, T. and Ohmura, A.: On the relationship between diurnal temperature range and surface solar radiation in Europe, J. Geophys. Res., 114, D00D07, doi:10.1029/2008JD011104, 2009.

Mallick, K., Jarvis, A., Fisher, J. B., Tu, K. P., Boegh, E. and Niyogi, D.: Latent Heat Flux and Canopy Conductance Based on Penman–Monteith, Priestley–Taylor Equation, and Bouchet's Complementary Hypothesis, Journal of Hydrometeorology, 14(2), 419–442, doi:10.1175/JHM-D-12-0117.1, 2013.

Mearns, L. O., Giorgi, F., McDaniel, L. and Shields, C.: Analysis of variability and diurnal range of daily temperature in a nested regional climate model: comparison with observations and doubled CO2 results, Climate Dynamics, 11(4), 193–209, doi:10.1007/BF00215007, 1995.

Mildrexler, D. J., Zhao, M. and Running, S. W.: A global comparison between station air temperatures and MODIS land surface temperatures reveals the cooling role of forests, Journal of Geophysical Research, 116(G3), doi:10.1029/2010JG001486, 2011.

Oyler, J. W., Dobrowski, S. Z., Holden, Z. A. and Running, S. W.: Remotely Sensed Land Skin Temperature as a Spatial Predictor of Air Temperature across the Conterminous United States, J. Appl. Meteor. Climatol., 55(7), 1441–1457, doi:10.1175/JAMC-D-15-0276.1, 2016.

Panwar, A., Kleidon, A. and Renner, M.: Do Surface and Air Temperatures Contain Similar Imprints of Evaporative Conditions?, Geophysical Research Letters, 46(7), 3802–3809, doi:10.1029/2019GL082248, 2019.

Price, J. C.: Estimation of Regional Scale Evapotranspiration Through Analysis of Satellite Thermal-infrared Data, IEEE Transactions on Geoscience and Remote Sensing, GE-20(3), 286–292, doi:10.1109/TGRS.1982.350445, 1982.

Renner, M., Wild, M., Schwarz, M. and Kleidon, A.: Estimating Shortwave Clear-Sky Fluxes From Hourly Global Radiation Records by Quantile Regression, Earth and Space Science, 6(8), 1532–1546, doi:10.1029/2019EA000686, 2019.

Rigden, A. J. and Li, D.: Attribution of surface temperature anomalies induced by land use and land cover changes: Attribution of Temperature Anomalies, Geophys. Res. Lett., 44(13), 6814–6822, doi:10.1002/2017GL073811, 2017.

Ronda, R. J., de Bruin, H. A. R. and Holtslag, A. A. M.: Representation of the Canopy Conductance in Modeling the Surface Energy Budget for Low Vegetation, Journal of Applied Meteorology, 40(8), 1431–1444, doi:10.1175/1520-0450(2001)040<1431:ROTCCI>2.0.CO;2, 2001.

Saltzman, B. and Pollack, J. A.: Sensitivity of the Diurnal Surface Temperature Range to Changes in Physical Parameters, Journal of Applied Meteorology, 16, 614–619, doi:https://doi.org/10.1175/1520-0450(1977)016<0614:SOTDST>2.0.CO;2, 1977.

Shukla, J. and Mintz, Y.: Influence of Land-Surface Evapotranspiration on the Earth's Climate, Science, 215(4539), 1498–1501, doi:10.1126/science.215.4539.1498, 1982.

Shuttleworth, W. J., Gurney, R. J., Hsu, A. Y. and Ormsby, J. P.: FIFE: the variation in energy partition at surface flux sites., IAHS Publ 186, no. 6, 1989.

Steduto, P. and Hsiao, T. C.: Maize canopies under two soil water regimes., Agricultural and Forest Meteorology, 89(3–4), 169–184, doi:10.1016/S0168-1923(97)00085-3, 1998.

Stenchikov, G. L. and Robock, A.: Diurnal asymmetry of climatic response to increased CO_2 and aerosols: Forcings and feedbacks, J. Geophys. Res., 100(D12), 26211, doi:10.1029/95JD02166, 1995.

Su, H., Wood, E. F., Mccabe, M. F. and Su, Z.: Evaluation of Remotely Sensed Evapotranspiration Over the CEOP EOP-1 Reference Sites, Journal of the Meteorological Society of Japan, 85A, 439–459, doi:10.2151/jmsj.85A.439, 2007.

Tang, B., Zhao, X. and Zhao, W.: Local Effects of Forests on Temperatures across Europe, Remote Sensing, 10(4), 529, doi:10.3390/rs10040529, 2018.

Thom, A. S.: Momentum, mass and heat exchange of vegetation, Quarterly Journal of the Royal Meteorological Society, 98(415), 124–134, doi:10.1002/qj.49709841510, 1972.

Thornthwaite, C. W.: An Approach toward a Rational Classification of Climate, Geographical Review, 38(1), 55, doi:10.2307/210739, 1948.

T.R., O.: Boundary layer climates, Routledge., 2002.

Tramontana, G., Jung, M., Camps-Valls, G., Ichii, K., Raduly, B., Reichstein, M., Schwalm, C. R., Arain, M. A., Cescatti, A., Kiely, G., Merbold, L., Serrano-Ortiz, P., Sickert, S., Wolf, S. and Papale, D.: Predicting carbon dioxide and energy fluxes across global FLUXNET sites with regression algorithms, , doi:10.5194/bg-2015-661, n.d.

Vinukollu, R. K., Wood, E. F., Ferguson, C. R. and Fisher, J. B.: Global estimates of evapotranspiration for climate studies using multi-sensor remote sensing data: Evaluation of three process-based approaches, Remote Sensing of Environment, 115(3), 801–823, doi:10.1016/j.rse.2010.11.006, 2011.

Wang, K. and Dickinson, R. E.: Contribution of solar radiation to decadal temperature variability over land, Proceedings of the National Academy of Sciences, 110(37), 14877–14882, doi:10.1073/pnas.1311433110, 2013.

Wild, M.: From Dimming to Brightening: Decadal Changes in Solar Radiation at Earth's Surface, Science, 308(5723), 847–850, doi:10.1126/science.1103215, 2005.

Yao, Y., Liang, S., Cheng, J., Liu, S., Fisher, J. B., Zhang, X., Jia, K., Zhao, X., Qin, Q., Zhao, B., Han, S., Zhou, G., Zhou, G., Li, Y. and Zhao, S.: MODIS-driven estimation of terrestrial latent heat flux in China based on a modified Priestley–Taylor algorithm, Agricultural and Forest Meteorology, 171–172, 187–202, doi:10.1016/j.agrformet.2012.11.016, 2013.

Zhang, W., Huang, Y., Yu, Y. and Sun, W.: Empirical models for estimating daily maximum, minimum and mean air temperatures with MODIS land surface temperatures, International Journal of Remote Sensing, 32(24), 9415–9440, doi:10.1080/01431161.2011.560622, 2011.

Zhao, L., Lee, X., Smith, R. B. and Oleson, K.: Strong contributions of local background climate to urban heat islands, Nature, 511(7508), 216–219, doi:10.1038/nature13462, 2014a.

Zhao, L., Lee, X., Smith, R. B. and Oleson, K.: Strong contributions of local background climate to urban heat islands, Nature, 511(7508), 216–219, doi:10.1038/nature13462, 2014b.

Zhu, W., Lǘ, A. and Jia, S.: Estimation of daily maximum and minimum air temperature using MODIS land surface temperature products, Remote Sensing of Environment, 130, 62–73, doi:10.1016/j.rse.2012.10.034, 2013.

Appendix

Table A1 Abbreviation used

Symbol	Full form	Unit
σ	Stefan-Boltzmann constant	W m^{-2} K^{-4}
ρ	Density of the lower atmosphere	Kg m^{-3}
LE	Latent heat flux	W m^{-2}
H	Sensible heat flux	W m^{-2}
G	Ground heat flux	W m^{-2}
DT_sR	Diurnal surface temperature range	K
DTR	Diurnal temperature range	K
DT_aR	Diurnal air temperature range	K
$(\overline{T_s - T_a})'$	Derivative of $\overline{T_s - T_a}$ to evaporative fraction	K
T_s	Surface temperature, obtained from longwave radiation	K
T_{ref}	Reference temperature	K
T_a	2 m air temperature	K
R_s	Surface solar radiation	W m^{-2}
$R_{s,max}$	Maximum of surface solar radiation	W m^{-2}
R_o	Net radiation at reference temperature	W m^{-2}
$R_{l,net}$	Net longwave radiation	W m^{-2}
k_r	Linearized constant	W m^{-2} K^{-1}
g_a	Aerodynamic conductance	m s^{-1}
f_e	Evaporative fraction	-

$\dfrac{dT_s}{dR_s}$	Surface temperature warming rate	K (W m^{-2})$^{-1}$
$\dfrac{dT_a}{dR_s}$	Air temperature warming rate	K (W m^{-2})$^{-1}$
$\dfrac{dg_a}{dR_s}$	Morning (20 W m^{-2} ≤ R$_s$ ≤ R$_{s,max}$) derivative of aerodynamic conductance to solar radiation	m s^{-1} /W m^{-2}
c_p	Specific heat capacity of the lower atmosphere	J/kg K
$\overline{T_s - T_a}$	Morning (20 W m^{-2} ≤ R$_s$ ≤ R$_{s,max}$) mean surface and air temperature gradient	K
$\overline{g_a}$	Morning (20 W m^{-2} ≤ R$_s$ ≤ R$_{s,max}$) mean aerodynamic conductance	m s^{-1}
$\left(\dfrac{dT_s}{dR_s}\right)'$	Derivative of surface temperature warming rate to evaporative fraction	K (W m^{-2})$^{-1}$
$\left(\dfrac{dT_a}{dR_s}\right)'$	Derivative of air temperature warming rate to evaporative fraction	K (W m^{-2})$^{-1}$

Table A2 Description of sites used for this study

Site no.	IGBP land use	Site ID	Site name	Location		Number of days used	DOI
				Latitude	Longitude		
1	Croplands (CRO)	AU-Rig	Riggs Creek	-36.65	145.57	237	https://doi.org/10.18140/FLX/1440202
2		CH-Oe1	Oensingen1 grass	47.28	7.73	182	https://doi.org/10.18140/FLX/1440135
3		CZ-wet	CZECHWET	49.02	14.77	184	https://doi.org/10.18140/FLX/1440145
4		DE-Geb	Gebesee	51.10	10.91	285	https://doi.org/10.18140/FLX/1440146
5		IT-BCi	Borgo Cioffi	40.52	14.95	274	https://doi.org/10.18140/FLX/1440166
6		IT-CA2	Castel d`Asso2	42.37	12.02	143	https://doi.org/10.18140/FLX/1440231
7		JP-SMF	Seto Mixed Forest Site	35.25	137.06	164	https://doi.org/10.18140/FLX/1440239
8		US-ARM	ARM Southern Great Plains site	36.60	-97.48	648	https://doi.org/10.18140/FLX/1440066
9	Croplands /Natural Vegetation (CRO/N	CH-Cha	Chamau grassland	47.21	8.41	188	https://doi.org/10.18140/FLX/1440131
10		CH-Fru	Fruebuel grassland	47.11	8.53	260	https://doi.org/10.18140/FLX/1440133

11	V)	FR-LBr	Le Bray (after 6/28/1998)	44.71	-0.76	265	https://doi.org/10.18140/FLX/1440163
12		US-Goo	'Goodwin Creek'	34.25	-89.87	206	https://doi.org/10.18140/FLX/1440070
13	Grasslands (GRA)	AU-Stp	Sturt Plains	-17.15	133.35	532	https://doi.org/10.18140/FLX/1440204
14		IT-MBo	Monte Bondone	46.01	11.04	480	https://doi.org/10.18140/FLX/1440170
15		US-AR1	ARM USDA UNL OSU Woodward Switchgrass 1	36.42	-99.42	242	https://doi.org/10.18140/FLX/1440103
16		US-AR2	ARM USDA UNL OSU Woodward Switchgrass 2	36.63	-99.59	225	https://doi.org/10.18140/FLX/1440104
17		US-SRG	Santa Rita Grassland	31.78	-110.82	696	https://doi.org/10.18140/FLX/1440114
18		US-Wkg	Walnut Gulch Kendall Grasslands	31.73	-109.94	1074	https://doi.org/10.18140/FLX/1440097
19	Shrublands (SH)	AU-ASM	Alice Springs	-22.28	133.24	477	https://doi.org/10.18140/FLX/1440194
20		US-SRC	Santa Rita Creosote	31.90	-110.83	621	https://doi.org/10.18140/FLX/1440098
21		US-SRM	Santa Rita Mesquite	31.82	-110.86	1121	https://doi.org/10.18140/FLX/1440090
22		US-Whs	Walnut Gulch Lucky Hills Shrubland	31.74	-110.05	558	https://doi.org/10.18140/FLX/1440097
23		AU-Cpr	Calperum	-34.00	140.58	284	https://doi.org/10.18140/FLX/1440195
24	Savannas (SA)	AU-DaP	Daly River Pasture	-14.06	131.31	439	https://doi.org/10.18140/FLX/1440123
25		AU-DaS	Daly River Savanna	-14.15	131.38	504	https://doi.org/10.18140/FLX/1440122
26		AU-Dry	Dry River	-15.25	132.37	466	https://doi.org/10.18140/FLX/1440197
27		AU-How	Howard Springs	-12.49	131.15	355	https://doi.org/10.18140/FLX/1440125
28	Woody Savannas (WSA)	AU-Gin	Gingin	-31.37	115.65	212	https://doi.org/10.18140/FLX/1440199
29		AU-Whr	Whroo	-36.67	145.02	206	https://doi.org/10.18140/FLX/1440206
30		IT-Noe	Sardinia/Arca di Noe	40.60	8.15	555	https://doi.org/10.18140/FLX/1440171

31		US-Me6	Metolius New Young Pine	44.32	-121.60	270	https://doi.org/10.18140/FLX/1440099
32		US-Var	Vaira Ranch	38.40	-120.95	1091	https://doi.org/10.18140/FLX/1440094
33	Deciduous Broadleaf Forest (DBF)	DK-Sor	Soroe- LilleBogeskov	55.48	11.64	169	https://doi.org/10.18140/FLX/1440155
34		IT-Col	Collelongo- Selva Piana	41.84	13.58	343	https://doi.org/10.18140/FLX/1440167
35		US-Oho	Oak Openings	41.55	-83.84	408	https://doi.org/10.18140/FLX/1440088
36		US-WCr	Willow Creek	45.80	-90.07	237	https://doi.org/10.18140/FLX/1440095
37	Evergreen Broadleaf Forest	AU-Wom	Wombat	-37.42	144.09	180	https://doi.org/10.18140/FLX/1440207
38	Evergreen Needleleaf Forest (ENF)	CA-Obs	SK-Southern Old Black Spruce	53.98	-105.11	620	https://doi.org/10.18140/FLX/1440044
39		CA-Qfo	Quebec Eastern Old Black Spruce (EOBS)	49.69	-74.34	194	https://doi.org/10.18140/FLX/1440045
40		DE-Tha	Tharandt- Anchor Station	50.96	13.56	268	https://doi.org/10.18140/FLX/1440152
41		IT-Lav	Lavarone (after 3/2002)	45.95	11.28	557	https://doi.org/10.18140/FLX/1440169
42		IT-Ren	Renon/Ritten (Bolzano)	46.58	11.43	362	https://doi.org/10.18140/FLX/1440173
43		NL-Loo	Loobos	52.16	5.74	401	https://doi.org/10.18140/FLX/1440178
44		US-GLE	GLEES	41.36	-106.23	514	https://doi.org/10.18140/FLX/1440069
45		US-Me2	Metolius Intermediate Pine	44.45	-121.55	450	https://doi.org/10.18140/FLX/1440079
46		US-NR1	Niwot Ridge (LTER NWT1)	40.03	-105.54	600	https://doi.org/10.18140/FLX/1440087
47	Mixed Forest (MF)	CA-Gro	ON-Groundhog River Mixedwood	48.21	-82.15	339	https://doi.org/10.18140/FLX/1440034
48		CA-Oas	SK-Old Aspen	53.62	-106.19	688	https://doi.org/10.18140/FLX/1440043
49		CA-TP4	ON-Turkey Point 1939 White Pine	42.70	-80.35	482	https://doi.org/10.18140/FLX/1440053
50		FR-Pue	Puechabon	43.74	3.59	535	https://doi.org/10.18140/FLX/1440164
51		RU-	Fedorovskoje-drained	56.46	32.92	257	https://doi.org/10.18140/FLX/1440

		Fyo	spruce stand				183

Observational analysis for each site
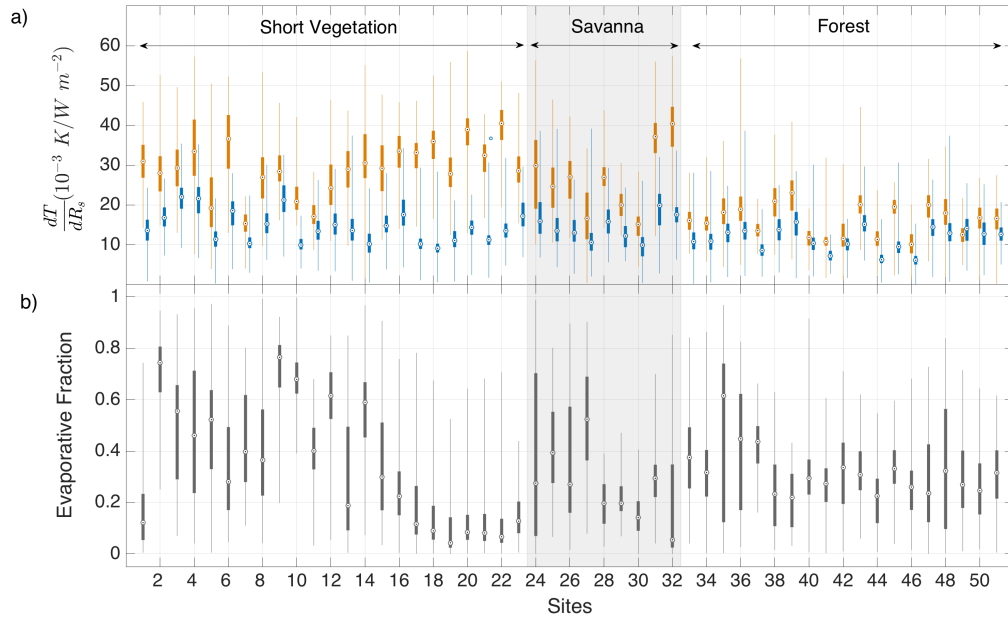
Figure A1 (a) Box plot of surface (T_s, orange) and air (T_a, blue) temperature warming rates (dT/dR_s), (b) Box plot of evaporative fractions. The vegetation types are separated by grey and white shades. The circle in the box plot indicates the median and the top and bottom edges indicate the 75th and 25th percentiles, respectively. The whisker covers the range in the observation.
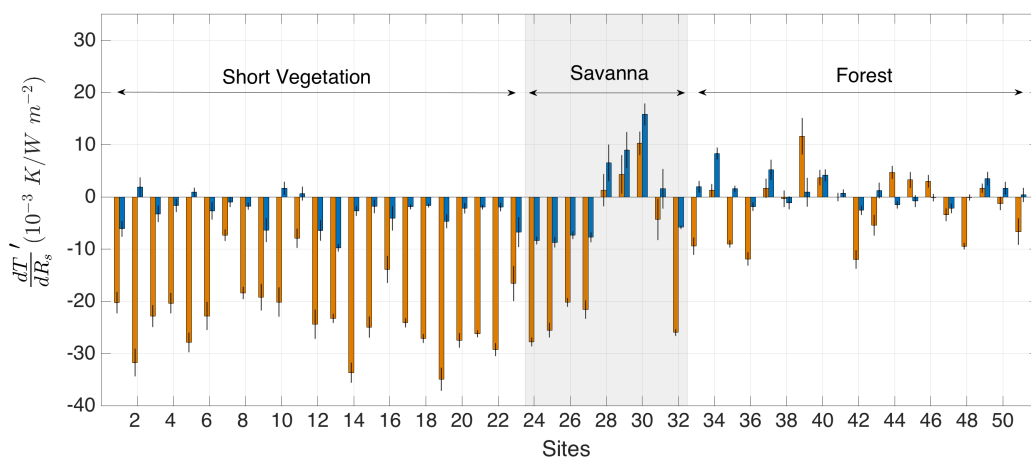
Figure A2 Warming rates response to evaporation, $(dT/dR_s)'$, for surface (T_s, orange) and air (T_a, blue) temperature. The vegetation types are separated by grey and white shades. The black bar represents the standard error in the linear regression of observed warming rate and evaporative fraction.
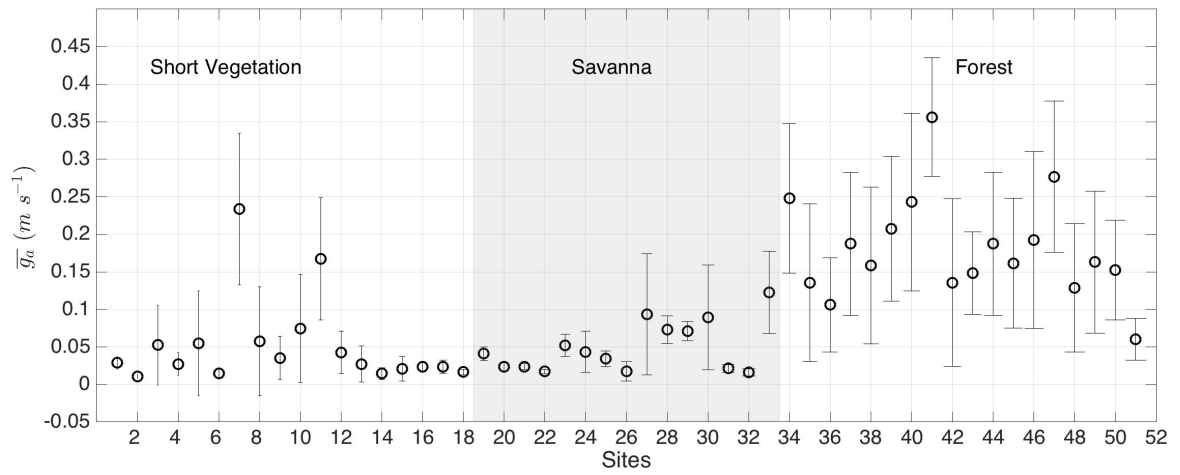
Figure A3 Morning time mean of aerodynamic conductance (g_a) for each site. The vegetation types are separated by grey and white shades. The error bar represents the standard deviation of the mean.